Articles

Modulating Dipoles for Structure−Function Correlations in the Gramicidin A Channel†

Myriam Cotten,‡,§ Changlin Tian,‡,|| David D. Busath,⊥ Randall B. Shirts,@ and T. A. Cross*,‡,§,||

Center for Interdisciplinary Magnetic Resonance at the National High Magnetic Field Laboratory, Department of Chemistry, and Institute of Molecular Biophysics, Florida State University, Tallahassee, Florida 32310, and Department of Zoology and Department of Chemistry, Brigham Young University, Provo, Utah 84602

Received December 18, 1998; Revised Manuscript Received May 3, 1999

ABSTRACT: Dipoles of the tryptophan indole side chains have a direct impact on ion conductance in the gramicidin channel. Here, fluorination of the indoles (both 5- and 6-fluoro) is used to manipulate both the orientations and the magnitudes of the dipoles. The orientations and positions with respect to the channel axis were determined using ^{2}H solid state NMR of uniformly aligned lipid bilayer preparations. By exchange of the remaining four protons in the indole ring for deuterium, comparison could be made to d_5-indole spectra that have previously been recorded for each of the four indoles of gramicidin A. After making the assignments which were aided by the observation of ^{19}F−^{2}H dipolar interactions, we found that fluorination caused only minor changes in side chain conformation. With the high-resolution structural characterization of the fluorinated indoles in position 11, 13, and 15, the electrostatic interactions with a cation at the channel and bilayer center can be predicted and the influence of the modified dipoles on ion conductance estimated. The importance of the long-range electrostatic interaction was recently documented with the observation of α-helical dipoles oriented toward the bilayer center on the ion conductance pathway for the *Streptomyces* K^+ channel. We present direct measurements of the orientation of gramicidin channel F-Trp positions for use in analysis of dipole effects on channel permeation.

The low-dielectric environment of the lipid bilayer provides unique opportunities for weak electrostatic interactions to play fundamentally important roles in protein function. Yet, the accuracy required for calculating such interactions is dependent on achieving very high-resolution molecular structure, such as can be achieved with solid state NMR-derived orientational constraints. Here, the influence of dipoles borne by modified indoles is characterized in the gramicidin monovalent cation selective channel. Both solid state NMR and single-channel conductance measurements are used to make the structure−function correlations.

Ion transport in membrane channels is dependent on the existence of electrostatic interactions between the ion and the channel in overcoming the high energy barrier due to the low dielectric constant of the bilayer. Monopole−dipole interactions provide much of this interaction energy. The origin of the dipoles appears to vary from channel to channel, confirming that the individual components should not be solely considered fundamental entities but rather participants in a common goal. In the potassium channel, four transmembrane α-helix dipoles have their negative ends pointing toward the cation pathway at the bilayer center (*1*). In gramicidin A, the dipoles are provided by the tryptophan (Trp) side chains (*2*).

The electric fields from the Trp side chains in the permeation pathway of the gramicidin channel depend on the magnitude and orientation of the heterocycle indole side chain dipole potential. The dipole moment of indole as a model compound has been measured on several occasions in benzene (2.05−2.11 D) (*3*−*5*) and in dioxane (2.38 D) (*6*). Furthermore, the orientation of the dipole has also been determined to form an angle of 50 ± 5° with the inter-ring bond, the positive end projecting toward the NH (*5*). In addition, the dipole moments of 5- and 6-fluoroindole have been measured in benzene (3.64 and 2.86 D, respectively) (*5*). No experimental estimate for the dipole angle for fluorinated indoles is available to our knowledge; however, the dipole angle should approximately follow the N−F orientation, and therefore, this angle should increase for 6-fluoroindole, and remain almost unchanged for 5-fluoroindole compared to that of indole. Crystal structures of fluorinated indole-3-acetic acid (IAA) exhibit little covalent bond length and angle variation for the various fluorinated analogues compared to the nonfluorinated IAA (*7*). For this study, it is assumed that the indole geometry is unchanged.

Computations of the magnitude and orientation of ground state dipoles have previously been performed using ab initio molecular orbital methods at the STO-3G, 4-31G*, and

† This work has been supported by National Institutes of Health Grant AI-23007, and the work was largely performed at the National High Magnetic Field Laboratory, which is supported by National Science Foundation Cooperative Agreement DMR-9527035 and the State of Florida.

‡ Center for Interdisciplinary Magnetic Resonance at the National High Magnetic Field Laboratory, Florida State University.

§ Department of Chemistry, Florida State University.

|| Institute of Molecular Biophysics, Florida State University.

⊥ Department of Zoology, Brigham Young University.

@ Department of Chemistry, Brigham Young University.

10.1021/bi982981m CCC: $18.00
Published on Web 06/30/1999

6-31G* basis set levels for indole (*5*, *8*, *9*) and derivatives (*8*−*11*), including the 4-, 5-, and 6-fluoroindoles (*9*) and tryptophan (*12*). Convergence of the partial charge distribution with a higher basis set level suggests that the higher basis set values are sufficiently accurate. To further verify this, we have carried out ab initio computations at the Hartree−Fock 6-311G** level for indole and 4-, 5-, and 6-fluoroindole, confirming basis set convergence.

It should be noted that there are numerous methods for determining partial atomic charges for molecules, e.g., Mullikan population analysis (*13*), natural bond orbital analysis (*14*), least-squares fitting of the electrostatic field (*15*), least-squares fitting with restraints (*16*), and electronegativity equalization methods (*17*, *18*). We believe the least-squares fitting of the electrostatic potential not only will give a set of charges consistent with the overall dipole moment (typically to within 1−2%), but also will give the best description of the electrostatic forces felt by nearby atoms. An effect not included in this kind of analysis, however, is the polarization of the molecule by nearby ions, polar solvent, or other molecules.

Gramicidin A (gA),[1] a major synthetic product of *Bacillus brevis*, is a 15-amino acid polypeptide that contains four tryptophan residues. The alternating D and L amino acid sequence induces the backbone to adopt a β-strand structure. In lipid bilayers, the polypeptide forms a cation selective channel which has been determined at high resolution using solid state NMR (*19*, *20*). It features an amino-terminal to amino-terminal single-stranded dimer with each monomer folding into a right-handed hydrogen-bonded helix of 6.5 residues per turn with the backbone lining the 4 Å diameter pore. The channel state has also been studied in SDS micelles (*21*, *22*) where the backbone structure has the same fold as in the lipid bilayer, but some side chain conformations differ. For membrane proteins, tryptophan is almost exclusively located at the hydrophobic−hydrophilic interface of membrane proteins, and in gA, it has several roles: (1) the eight Trp side chains orient the dimeric channel (*23*) with respect to the bilayer normal; (2) they stabilize the single-stranded dimeric conformation (*23*−*32*); (3) they modulate key interactions with the lipids (*33*) and facilitate ion conductance (*2*, *23*, *29*, *34*, *35*); and (4) they may have an important role in defining the helical sense of the channel (*36*, M. Cotten et al., unpublished results).

Solid state NMR of site specifically ^{15}N-, ^{13}C-, and ^{2}H-labeled gramicidin A in lamellar phase bilayers has been used to determine the high-resolution structure (*2*, *19*, *20*, *23*). Orientational constraints derived from uniformly aligned samples constrain the orientation of individual nuclear sites with respect to the magnetic field axis. Numerous precise constraints have led to a well-defined structure. In particular, each of the indole rings in gA has been characterized by the anisotropic ^{15}N chemical shift, the ^{15}N−^{1}H dipolar interaction, and five ^{2}H quadrupolar splittings (*37*). On the basis of these accurate indole orientations with respect to the channel axis, Hu and Cross (*2*) have estimated electrostatic interactions between each indole and the cation at the bilayer center on the channel axis using the dielectric constant as a parameter. The conductance for gA and for all the sequence variants involving phenylalanine (no dipoles) instead of tryptophan was plotted semilogarithmically against the sum of the remaining dipole−monopole interactions. The linear correlation over a factor of 20 in conductance was consistent with the hypothesis that, under these conditions, the potential energy barrier at the channel center represents the rate-limiting step. More recently, Andersen et al. (*38*) performed conductance studies with two gA analogues containing both a 5-fluorotryptophan (5F-Trp) and a phenylalanine in place of two of the four tryptophans. Assuming similar dipole moment and side chain orientations for the 5F-Trp and Trp side chains at a given position, the authors correlated the increase in ion conductance upon replacement of Trp with 5F-Trp to enhanced dipole−monopole interactions.

In the study presented here, experimental evidence was sought to further support these functional roles of the Trp dipole moment. By substituting ^{2}H-labeled 5-fluorotryptophan and 6-fluorotryptophan (6F-Trp) for Trp in gA, we have obtained a collection of different dipole moment magnitudes and orientations that were expected to induce minimal structural effects in gramicidin. The ^{2}H and ^{15}N solid state NMR characterization in hydrated lipid bilayers of eight analogues containing ring-d_4 5F-Trp or 6F-Trp at positions 9, 11, 13, and 15 (d_4-5F-Trp gA or d_4-6F-Trp gA) and an ^{15}N amide label have confirmed this qualitative expectation. The ^{2}H quadrupolar splittings were used to constrain the dipole moment orientations. These results were then compared to those previously published (*2*) for the Trp side chains of ring-d_5-gA (d_5-gA). Direct comparison of the side chain dipole moments to measured channel conductances is beyond the scope of this paper. The electric fields of these dipoles and their use in kinetic modeling of the modified channel conductances will be presented elsewhere. However, an initial interpretation of the single-channel conductance recorded for the 5F-Trp$_{13}$-labeled gramicidin analogue (*35*) will be described, and some predictions for the functions of the other analogues will be offered.

MATERIALS AND METHODS

Ring-d_4-5F-Trp and ring-d_4-6F-Trp were purchased from Cambridge Isotope Laboratories (Woburn, MA). All other isotopically labeled amino acids were also purchased from Cambridge Isotope Laboratories. The gramicidin fluoro analogues were synthesized by solid phase peptide synthesis using Fmoc (9-fluorenylmethoxycarbonyl) chemistry on an Applied Biosystems model 430A peptide synthesizer. The blocking chemistry was performed in our lab. Details of the synthesis and blocking chemistry have been described previously (*39*, *40*). Once cleaved from the solid phase support, the peptides were characterized and the purity was assessed by HPLC (*39*, *40*).

Oriented samples for solid state NMR were prepared by codissolving gA or the fluoro analogues and dimyristoylphosphatidylcholine (DMPC) or dioleoylphosphatidylcholine (DOPC) in a 95/5 (v/v) benzene/ethanol solution. After a freeze−thaw cycle, the solution, while still cool, was spread on glass coverslips. Partial evaporation of the solvents

[1] Abbreviations: F-Trp, fluorinated tryptophan; 5F-Trp, (5-fluoroindole)tryptophan; 6F-Trp, (6-fluoroindole)tryptophan; d, deuterium; DMPC, dimyristoylphosphatidylcholine; DOPC, dioleoylphosphatidylcholine; DPhPc, diphytanoylphosphatidylcholine; gA, gramicidin A; Gly, glycine; HPLC, high-performance liquid chromatography; NMR, nuclear magnetic resonance; Phe, phenylalanine; qcc, quadrupolar coupling constant; rmsd, root-mean-square deviation; SDS, sodium dodecyl sulfate; Trp, tryptophan.

occurred at room temperature. The samples were then dried overnight under vacuum and stacked in a square glass tube before 50% HPLC-grade water was added (by total sample dry weight). The tubes were then sealed and incubated at 45 °C until the samples became transparent, uniformly hydrated, and oriented such that the bilayers were parallel to the glass slides. A shorter incubation was required for DOPC than for DMPC samples.

Solid state NMR spectra were acquired on a Bruker 600 MHz spectrometer with a resonance frequency of 92.1 MHz for ^{2}H NMR. A standard quadrupole echo pulse sequence with a 1 MHz sweep width, a 3.1 μs 90° pulse width, 22 μs echo delays, and a 0.4 s recycle delay was used. The spectral data were processed using UXNMR software (Bruker).

Data Analysis. When two sources for motional averaging of the quadrupolar splittings were taken into account, namely, the global rotation of gramicidin A about its helical axis and the side chain librational motions described by Hu et al. (*37*), the description of the orientational dependence of the indole quadrupolar splitting was given by

$$\Delta\nu = {}^3/_4\mathrm{qcc}(3\cos^2\theta - 1)[{}^1/_2(3\cos^2\beta - 1)] \quad (1)$$

where θ is the angle between the axis of motional averaging and a given C−D bond. β is the angle between the axis of motional averaging and the magnetic field. Since the axis of motional averaging is the gramicidin helical axis and bilayer normal, both aligned along the magnetic field direction in our experiments, θ becomes the angle between the magnetic field and the C−D bond, and β is equal to 0°. The value used for the quadrupolar coupling constant (qcc) was adjusted from its static value of 183 kHz to reflect local side chain motional averaging that has been previously characterized for gA (*37*).

For a computational search of χ_1 (C_α−C_β) and χ_2 (C_β−C_γ) conformational space, a program written within Maple software was used. The geometry of the indole was obtained from Biosym Technologies (Insight II software) and corresponds to coplanar five- and six-membered indole rings. The Trp and Trp analogue side chains with fixed C_α and C_β positions, given by the refined backbone structure of gA, were rotated about χ_1 and χ_2 in 5° increments. The quadrupolar splittings of the ring deuterons were obtained for each combination of χ_1 and χ_2 using eq 1. The root-mean-square deviations (rmsds) were calculated according to

$$\mathrm{rmsd} = \{[\sum(\Delta\nu_{\mathrm{cal}} - \Delta\nu_{\mathrm{obs}})^2]/n\}^{1/2} \quad (2)$$

where $\Delta\nu_{\mathrm{cal}}$ and $\Delta\nu_{\mathrm{obs}}$ are the calculated and observed quadrupolar splittings, respectively. The sum is made over the *n* deuterons of the ring (5 for Trp and 4 for the fluoro analogues), and the units are kilohertz.

For each reasonable assignment, a contour plot of the rmsd as a function of χ_1 and χ_2 was obtained using Gnuplot. The plot giving rise to the lowest rmsd was retained. The lower rmsds were found to correspond to one of the tentative assignments. The region of interest for this study was uniformly found to be from 270 to 305° for χ_1 and from 260 to 320° for χ_2. This region was refined using 1° increments for the rotations.

Calculations of Dipole Moment Orientations and Atomic Charges. Dipole moments and their vector components as well as partial atomic charges for indole, 5-fluoroindole, and 6-fluoroindole were calculated using the commercial program Spartan (release 4.1.2, Wavefunction, Inc., Irvine, CA) operating on Silicon Graphics O2 workstations. Calculations were carried out at the RHF-SCF 6-31G* and 6-311G** levels, and included calculations of the dipole moments from the SCF wave function. Atom-centered charges were determined using the Spartan elpot option which does a least-squares fit to the electrostatic potential generated by the wave function together with the nuclear charges at 5000−6000 points in the volume near the molecule but with points within the van der Waals radius of each atom excluded. These points effectively sample the region in which neighboring molecules in a membrane interact with the molecule in question. This level of calculation is considered to be very good, but is known in some instances to overestimate the dipole moment of molecules by as much as several percent; however, no attempt was made to scale the dipole moments to correct for this tendency because the overestimation is not accurately characterized for this class of compound or for relative errors in the different dipole vector components. In addition, in a hydrogen bonding solvent such as water, the amino acid side chains may be polarized by the solvent, so overestimating the charges may give a more realistic dipole moment in solvent than the true dipole moment in a vacuum. Calculated dipole moments agree with experimental ones to within 10%. In addition, dipole moments for RHF-SCF 6-311G** basis set differ by only 1−2% from those calculated using the RHF-SCF 6-31G* method, suggesting convergence in the size of the basis set.

In this calculation, the dipole moment of the tryptophan side chain has been approximated by the dipole moment of the isolated indole molecule. In other words, it has been assumed that the charge distribution of a given isolated indole or F-substituted indole molecule is not measurably changed when the peptide chain is substituted for the hydrogen atom at the indole 3 position. To some extent, this problem has been addressed here through a comparison of the partial charges of indole and 3-methylindole.

RESULTS

The electrostatic potential profile produced by the ab initio wave function has been fit by assigning partial charges to each atom. These charges reproduce the dipole moment to less than 1% error, including the individual components, which are used below to produce the axial, radial, and tangential dipole components (relative to the channel axis) of the gA side chains in their observed positions. The charges are also being used to compute the side chain electrostatic potential along the channel axis, which will be reported elsewhere.

The 6-311G** partial charges in Figure 1 are consistent with prior reports and from our 6-31G* calculations. Alagona et al. (*9*; G. Alagona personal communication) computed partial charges, dipole moments, and angles for indole and 5- and 6-fluoroindole using 6-31G* level computations. Our 6-31G* computations are consistent with those of Alagona and co-workers with the largest discrepancy being for 5-fluoroindole with values that differ by 0.30 D and 1.8°. Increasing the basis set level to 6-311G** had negligible effects on the dipole angles (<0.3°) and increased the dipole magnitude by ~0.1 D. Thus, it appears that the angle, which

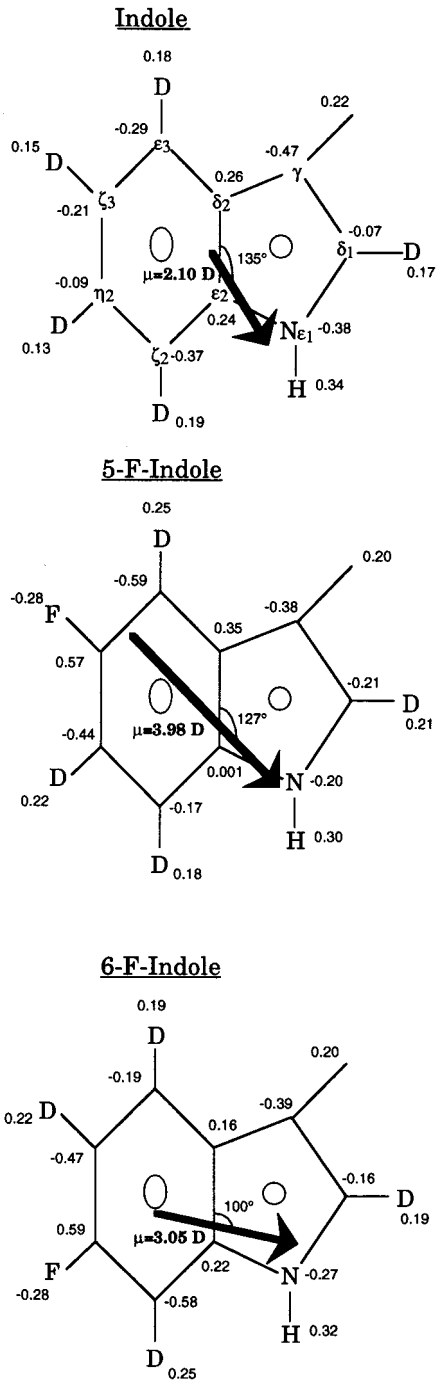

FIGURE 1: Chemical structures, dipole moments, and atomic charges of the indole and fluoro-substituted indoles used for the study. The chemical structures of d_5-indole and the two fluorinated analogues, d_4-5F-Trp and d_4-6F-Trp, are shown. The orientations of the calculated dipole moments with respect to the $C_{\delta_2}-C_{\epsilon_2}$ bond shared by the five- and six-membered rings are given. Atomic charges were taken from ab initio calculations for indole and fluroinated indoles. The label for the hydrogen attached to C3 (C_γ) is deleted to indicate the point of attachment to the C_β of methylene, but the partial charge of H at that position in indole is included for completeness.

is most important for our purposes, is very well converged and the dipole magnitude is satisfactory.

The partial charges are not as consistent from one approach to another, with the charges on the N and adjacent inter-ring C exhibiting the greatest variance between the Merz-Kollman fitting method (used in ref *9*) and that used here. Although the pattern of partial charges is quite consistent across basis sets, the charge magnitudes tend to strengthen and then converge with increased basis set size (*10*). For the 6-311G** method, the partial charge-based dipole moments are within 0.04 D of the ab initio dipole moments and angles are essentially identical for all four of the compounds that were studied. The 6-311G** partial charge-based dipoles and angles for indole, 5-fluoroindole, and 6-fluoroindole are also shown in Figure 1. The magnitudes are greater than the values measured in benzene (*5*) by 0.00, 0.34, and 0.19 D, respectively. The calculated angle for indole is lower than that measured by 5°, but within the experimental error bar of ±5°. For 5-fluoroindole, the dipole moment is almost doubled in magnitude compared to that of indole and its orientation differs by only 8°. In contrast, the dipole moment of 6-fluoroindole is increased by only 50% and its orientation is changed by 35°. Moreover, the partial charges on deuterons neighboring fluorine are significantly altered as are the partial charges on the heavy atoms throughout the ring system.

It has been noticed (*11*) that partial atomic charges fit using several hundred points (as in ref *9*) can exhibit a large degree of dependence on the precise choice of fitting points. This usually shows up in a dependence of the charges on the orientation of the entire molecule in space. Since we sampled the electrostatic potential at several thousand points rather than at only several hundred, we believe that our partial charges should exhibit a lower level of orientational sensitivity than previously reported charges. This could explain the discrepancy between our 5-fluoroindole dipole moment and that of Alagona et al. (*9*) mentioned above, as well as the difference in the fitted partial atomic charges.

Although we have not computed the charge distribution for Trp, comparison of our 6-31G* charges for indole to the 6-31G* partial charges for 3-methylindole (*11*), in which the 3-methyl simulates tryptophan's β-methylene, shows that all partial charges are within 0.10 except those on the methyl, C3, and the adjacent inter-ring carbon. Namely, the methyl group charge is lower than the indole C3 hydrogen by 0.155, the C3 charge higher by 0.391, and the adjacent inter-ring carbon charge lower by 0.233. The computed dipole moment for 3-methylindole is 1.941 D (*11*), similar to that computed by us for indole at the 6-31G* level. Because the dipole moments of indole and 3-methylindole are quite similar and the partial charge effects are localized at some distance from the fluorination sites, the consequences of the β-methylene in the Trp side chain can be neglected for our purposes here.

Figure 2 shows the ^2H spectra of oriented gA analogues in DMPC bilayers containing a d_4-5F- or d_4-6F-Trp at position 9 (A), 11 (B), 13 (C), and 15 (D). The top spectrum for each position is from Hu et al. (*37*) for d_5-Trp-labeled gramicidin A (gA) in DMPC bilayers. Typically, somewhat broader resonance lines were observed for the F-Trp-gA spectra. This broadening probably reflects an increased heterogeneity in side chain orientation with respect to the magnetic field. This feature that is especially true for 5F-Trp_9 is associated with the furthest penetration of fluorine into the bilayer with the analogues used in this study. The line width of the d_4-F-Trp_9 resonances has prevented a detailed structural analysis, restricting the study presented here to the other analogues at positions 11, 13, and 15. Even spectra obtained in DOPC (Figure 3A) did not exhibit better

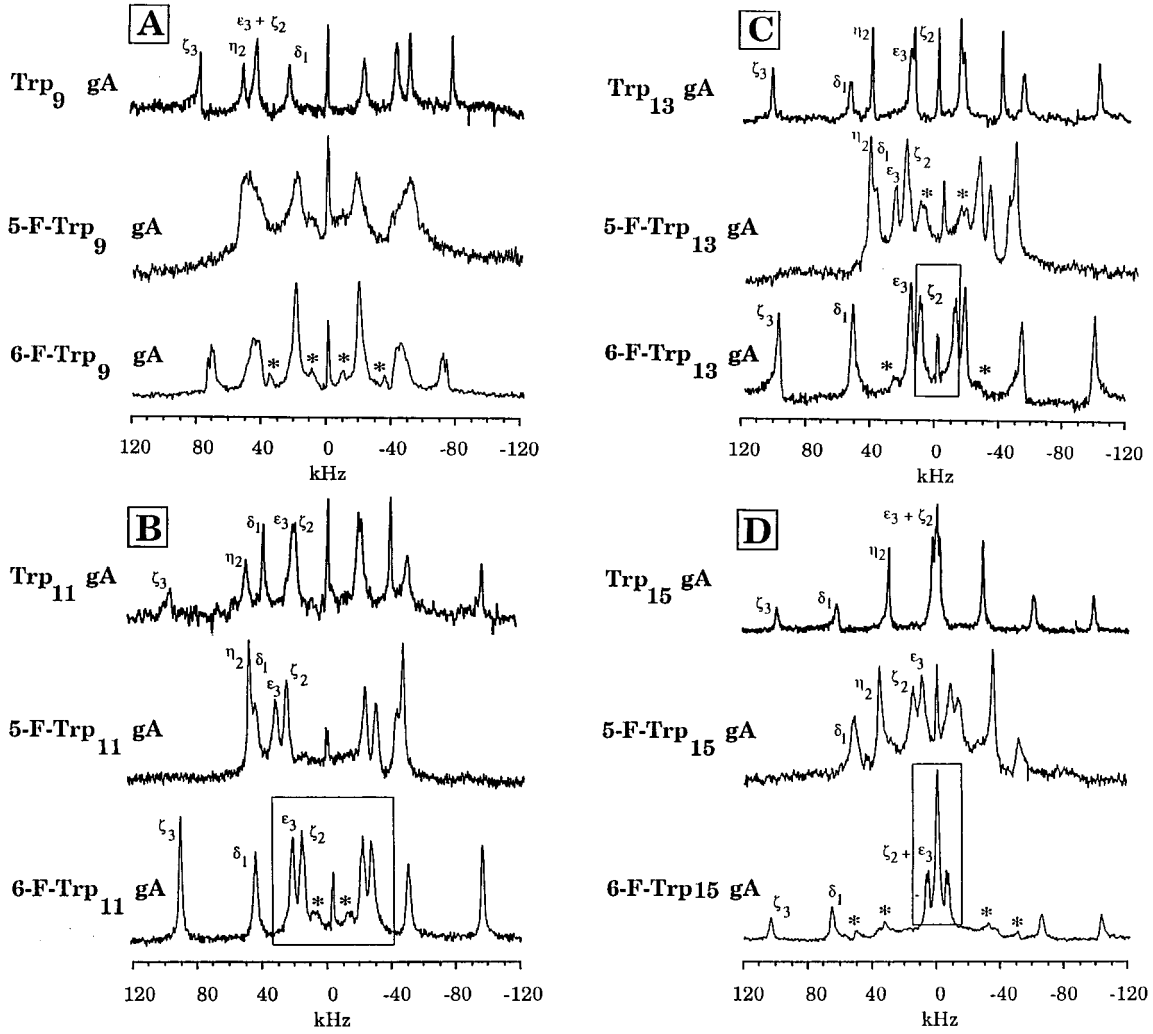

FIGURE 2: ^{2}H spectra of d_5-Trp-, d_4-5F-Trp-, and d_4-6F-Trp-labeled gramicidins in uniformly aligned DMPC bilayers (peptide to lipid molar ratio of 1:8). The spectra were recorded at 40 °C, above the gel to liquid-crystalline phase transition of the lipids. Data for positions 9, 11, 13, and 15 are depicted by sets labeled A−D, respectively. The top spectrum from each set is from gramicidin A (*37*). The middle and bottom spectra are from 5F-Trp-gA and 6F-Trp-gA, respectively. For positions 11, 13, and 15, the spectral resolution is adequate for distinguishing all expected splittings (five for Trp and four for the fluoro analogues), which can be used as high-resolution orientational constraints. In contrast, due to lower resolution at position 9, four splittings are observed in gA. In 5F-Trp-gA and 6F-Trp-gA, significantly broader lines prevent the determination of high-resolution orientational constraints. Selected regions shown in boxes have been enlarged in Figure 4. A high degree of similarity exists between the spectra at a given position. On the basis of the results of the data analysis (see the text), the resonances have been assigned to the ring deuterons using the nomenclature shown in Figure 1. Residual signals from unoriented portions of the samples have been marked with an asterisk, and residual HDO signals are observed at 0 kHz.

resolution for the d_4-F-Trp$_9$ resonances.

Despite the slight broadening of the resonances for d_4-F-Trp at positions 11, 13, and 15, substantial similarity exists between the d_5-Trp-gA spectra and those of its corresponding d_4-6F-Trp-gA analogue excepting, of course, the missing deuteron in each fluorinated analogue. Even for d_4-6F-Trp$_9$-gA, significant similarity exists. However, it is much more difficult to see similarities between d_5-Trp-gA and d_4-5F-Trp-gA, although when the resonances are assigned, it will be seen that most changes in the quadrupolar splittings are relatively small. This suggests, as will be strongly supported by the analysis, that both the ring orientations and their dynamics are similar in gA and these fluorinated analogues. One of the most striking differences between the d_5-Trp and d_4-F-Trp spectra is associated with the para deuterons of the six-membered ring. These two para C−^{2}H bonds (ϵ_3 and ζ_2) are almost parallel in the model compound crystal structure (*41*), and for d_5-Trp-gA, two quadrupolar splittings are almost identical. This means that the ^{2}H electric field gradient tensors are almost identical and have almost identical orientations with respect to the magnetic field axis. In the F-Trp-gA analogues, there is no pair of splittings that are consistently observed to be within a couple of kilohertz. The fluorine has either influenced the neighboring ^{2}H electric field gradient tensors significantly or affected the relative orientation of these para C−^{2}H bonds.

The initial assignments of the ^{2}H quadrupolar splittings were aided by spectra obtained in DOPC (Figure 3). To confirm that there is no significant change in the backbone structure, $^{15}N_\alpha$ chemical shifts from oriented samples of 5F-Trp-gA prepared in DOPC bilayers have been compared to values obtained in DMPC bilayers. On the basis of the results described above, it is anticipated that the most significant changes in the backbone would be induced by 5F versus 6F analogues. No significant changes have been observed with

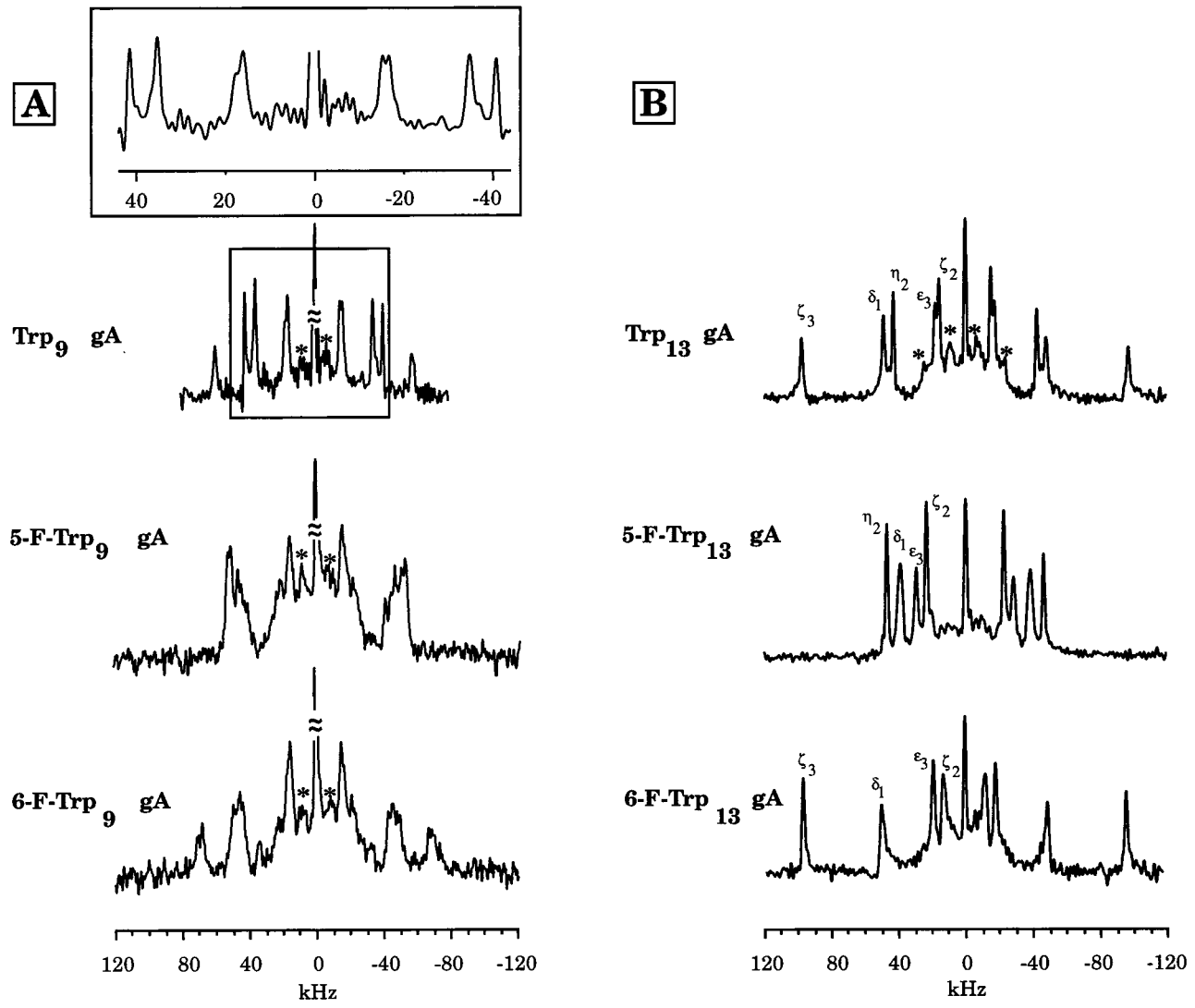

FIGURE 3: ^{2}H spectra of d_5-Trp, d_4-5F-Trp, and d_4-6F-Trp at positions 9 and 13 in gramicidin solubilized in uniformly aligned DOPC bilayers. The spectra were recorded at about 30 °C, above the gel to liquid-crystalline phase transition temperature of the lipids. (A) Position 9 is not greatly improved in DOPC (1:35 peptide to lipid molar ratio) vs DMPC (1:8 peptide to lipid molar ratio, Figure 2). The para deuterons in Trp$_9$-gA are still not resolved, but the expansion in the inset suggests a broader inner splitting. (B) At position 13 (1:25 peptide to lipid molar ratio), all expected splittings (five for Trp and four for the fluoro analogues) are identified and assigned as described in the legend of Figure 2, and explained in the text. The number of scans varied from 50 000 to 150 000.

Table 1: Comparison of ^{15}N Backbone Chemical Shifts for the Gramicidin A Channel and Fluorotryptophan Gramicidins

	$^{15}N_\alpha$ chemical shift (ppm) in DMPC			
^{15}N label site	gA	5F-Trp$_9$-gA	5F-Trp$_{13}$-gA	5F-Trp$_{15}$-gA
Gly$_2$	113		113	
Trp$_{11}$	185	185		
Leu$_{12}$	133		133	
Trp$_{13}$	182			181
	$^{15}N_\alpha$ chemical shift (ppm) in DOPC			
^{15}N label site	gA		5F-Trp$_{13}$-gA	5F-Trp$_{15}$-gA
Gly$_2$	113		111	
Leu$_{12}$			133	
Trp$_{13}$			176	180

5F-Trp$_9$-, 5F-Trp$_{13}$-, or 5F-Trp$_{15}$-gA incorporated into either DMPC or DOPC (Table 1). Therefore, it is reasoned for the interpretation of the side chain quadrupolar splittings that the backbone structure is unchanged in either DOPC or DMPC upon the substitution of a fluorinated indole.

The ^{2}H quadrupolar spectra of Trp$_{13}$-gA analogues in DOPC bilayers are shown in Figure 3B. The resolution is as good if not better than in DMPC, and the quadrupolar splittings, as well as those from Figure 2, are presented in Table 2. The splitting assignments for positions 11, 13, and 15 of d_5-Trp-gA have been established through the use of $^{15}N_{\epsilon_1}$ chemical shifts and $^{15}N_{\epsilon_1}-^1$H dipolar results. Here we do not have the $^{15}N_{\epsilon_1}$ data, but it is clear that the 195 kHz splitting in 6F-Trp$_{13}$-gA and Trp$_{13}$-gA in DOPC, the 198 kHz splitting in 6F-Trp$_{13}$-gA in DMPC, and the 204 kHz splitting in Trp$_{13}$-gA in DMPC are consistent with the absence of this large splitting when the 5F-Trp analogue is incorporated, and hence, these splittings are assigned to the ζ_3 site. Expansions of the 6F-Trp-gA spectra from Figure 2 are shown in Figure 4. Present in the spectra of these fluorinated analogues are $^{19}F-^2$H dipolar splittings. The magnitude of these splittings is dependent on both the distance between nuclei and the orientation of the internuclear vector with respect to the magnetic field axis. On the basis of the Trp-gA indole orientations, the only $^{19}F-^2$H dipolar interaction

Table 2: ^{2}H Splitting for the Indole Rings and Fluorinated Tryptophans in Gramicidin A and Fluoro Analogues

	DMPC					
	Trp_{11}	5F-Trp_{11}	6F-Trp_{11}	Trp_{13}	5F-Trp_{13}	6F-Trp_{13}
δ_1	77	84	96	108	90	108
ϵ_3	43	60	49	−32	−58	−34
ζ_2	39	46	38	−28	−44	−22
ζ_3	192		189	204		198
η_2	−99	−90		−81	−82	

	DMPC		
	Trp_{15}	5F-Trp_{15}	6F-Trp_{15}
δ_1	123	104	132
ϵ_3	−4	18	−1
ζ_2	−1	30	−12
ζ_3	198		207
η_2	−59	−72	

	DOPC		
	Trp_{13}	5F-Trp_{13}	6F-Trp_{13}
δ_1	97	77	100
ϵ_3	−35	−58	−38
ζ_2	−31	−46	−27
ζ_3	195		195
η_2	−85	−93	

that would be large enough to be resolved in the observed spectra is that from 6F-Trp $^2H_{\zeta_2}$. Therefore, the ±12 kHz quadrupolar splitting from 6F-Trp_{15}, the ±22 kHz splitting from 6F-Trp_{13}, and even the ±38 kHz splitting of 6F-Trp_{11} (despite no well-resolved $^{19}F-^2H$ dipolar splitting) have been assigned to the ζ_2 deuteron in DMPC environments. Moreover, by analogy, and because of a broader line width, the ±27 kHz splitting in 6F-Trp_{13} in DOPC has been assigned to this deuteron. The smallest splitting in 5F-Trp_{13} is 44 kHz, and it is tentatively assigned to ζ_2 as well. The other para deuteron, ϵ_3, is assigned to the most similar splitting, ±34 kHz for 6F-Trp_{13} in DMPC, ±38 kHz for 6F-Trp_{13} in DOPC, and ±58 kHz in 5F-Trp_{13}. The remaining deuteron in 6F-Trp_{13}, δ_1, is assigned to the 108 kHz splitting in DMPC and to the 100 kHz splitting in DOPC, similar to the same assignment of the 108 kHz splitting in the DMPC sample of gA. The remaining initial assignment of the η_2 and δ_1 deuterons in 5F-Trp_{13}-gA is not very reliable, but the δ_1 deuteron is relatively close to the N_{ϵ_1} proton and C_β protons, leading to a broad resonance (due to $^2H-^1H$ dipolar coupling) as seen in the 5F-Trp spectrum in DMPC at 82 kHz and in the 77 kHz splitting in DOPC. For Trp_{11} and Trp_{15}, similar rationales for the tentative assignments exist.

To finalize the assignments and constrain the orientation of the rings with respect to the channel axis by taking into account all of the NMR orientational constraints, a computational search of χ_1 and χ_2 conformational space was performed as described in Materials and Methods. Here the root-mean-square deviation (rmsd, in kilohertz) between calculated and observed quadrupolar splittings is computed for each ring as a function of the χ_1 and χ_2 angles. In this process, the quadrupolar splittings that are less than half-maximal were analyzed with both positive and negative signs. Furthermore, the motionally averaged tensors for the deuterons in the analogues were assumed to be the same as that for gA (*37*). This assumption is made despite concerns over the influence of fluorine and will be revisited after the analysis. The plots for gA have been recalculated using only

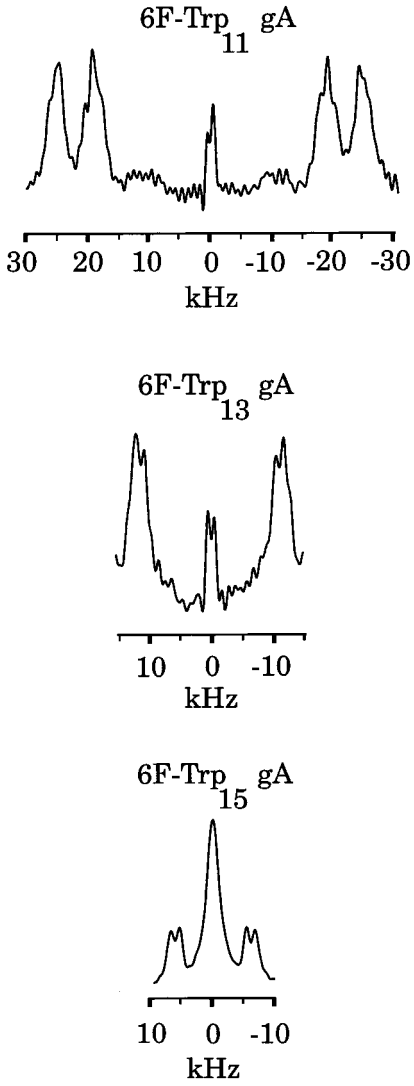

FIGURE 4: Expanded regions corresponding to the boundaries of the boxes in Figure 2. 6F-Trp_{13} and 6F-Trp_{15} side chains clearly display a split of one pair of resonances of the para deuterons due to the $^{19}F-^2H$ dipolar interaction. This has been used to assign this resonance to the para deuteron closest to the fluorine, $^2H_{\zeta_2}$. For the same reason, the broadened inner splitting in 6F-Trp_{11} has been assigned to $^2H_{\zeta_2}$.

the quadrupolar splittings from Hu et al. (*37*) so that all maps could be compared on the basis of (1) the same type of orientational constraints and experimental errors and (2) the same backbone structure. The 1995 study (*37*) used the Ketchem et al. (*19*) backbone structure, whereas this analysis uses the refined structure in the Protein Data Bank (file name 1mag) (*20*).

In the process of redoing these conformational plots for gA, the assignments of the para deuterons came into question. Small ^2H splitting values as seen for the para deuterons in gA in DMPC indicate that the $\cos^2\theta - 1$ term in eq 1 is small, and therefore, θ is close to the magic angle ($\theta_m = 54.7°$). A small change of θ in this range not only can substantially change the magnitude of the splitting but also can change the sign of the splitting. Indeed, Trp_{15} and 5F-Trp_{15} splittings in DMPC have similar absolute magnitudes for the para deuterons, but conformational space analysis clearly showed opposite signs. The sign of a quadrupolar splitting is not known unless its magnitude is larger than

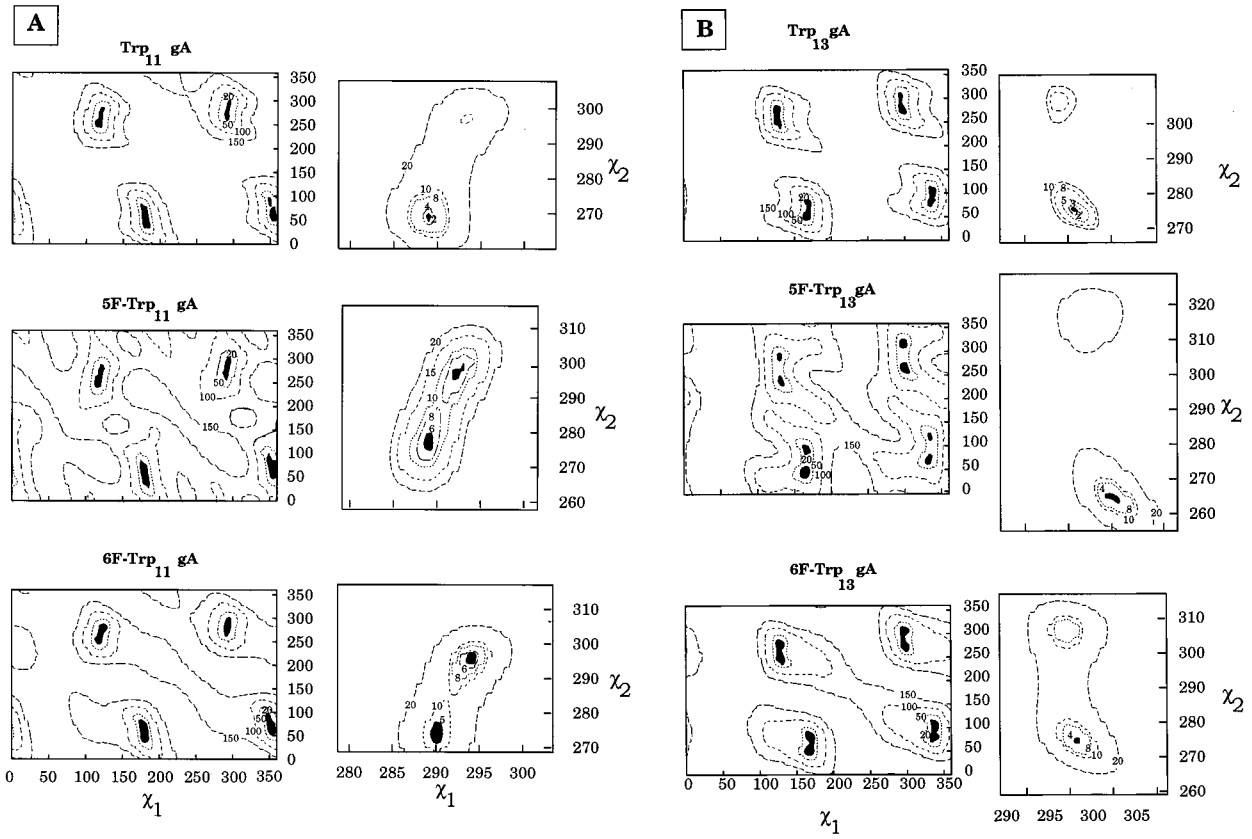

FIGURE 5: Contour plots of the minimal root-mean-square deviation (rmsd, in units of kilohertz) between the observed quadrupolar constraints and the calculated observables based on χ_1 and χ_2 angles for Trp, 5F-Trp, and 6F-Trp side chains at positions 11 (A) and 13 (B) in DMPC. The entire conformational space has been searched in increments of 5° as shown in the first set of maps (0 to 360°, left side of the figure). The rmsd values for the contours are indicated in the maps. The minima having χ_1 values near 180 and 300° are close to two χ_1 and χ_2 rotameric states for tryptophan. The two other regions, having χ_1 values near 120 and 340°, correspond to $N_{\epsilon_1}-H$ bond orientations pointing toward the center of the bilayer, which is inconsistent with the channel function of gramicidin. The region of interest for this study corresponds to χ_1 values near 300° based on functional considerations and Raman data, and has been extracted for refinement in 1° increments as shown in the second set of maps for each side chain.

$^3/_4$qcc, in which case it is positive (see eq 1). The negative signs for the splittings of the para deuterons of Trp_{13}- and Trp_{15}-gA represent corrections to the original sign assignment by Hu et al. (*37*).

The plots corresponding to the full χ_1 and χ_2 conformational space from 0 to 360° performed with 5° increments have four minima. Two of these regions having χ_1 values of around 170 and 300° also appear in the maps obtained by Hu et al. (*37*), but the other two regions with χ_1 values of near 120 and 340° did not appear. This is because of the additional ^{15}N chemical shift and $^{15}N-^1H$ dipolar constraints used in the study by Hu et al. (*37*). Since the maps in the study presented here are otherwise so similar to those of Hu et al. (*37*) and as noted by Koeppe et al. (*42*), those regions near 120 and 340° correspond to N−H orientations pointing toward the center of the bilayer, these regions have been excluded from further consideration.

Furthermore, it was argued by Hu and Cross (*2*) on the basis of functional and energetic arguments that the χ_1 region near 300° was the most probable region. This conformation belongs to low-energy regions characterized by Dorigo et al. (*43*) based on energetic arguments about conformational energy in gA. Therefore, the study presented here has focused on this conformational space, and the contour plots have been refined using 1° increments in both χ_1 (280−305°) and χ_2 (260−320°) dimensions. Figure 5 shows such maps for gA, 5F-Trp-gA, and 6F-Trp-gA at positions 11 and 13 in DMPC. The local minima are depicted as blackened areas. The rmsd values for Trp-gA are very small, confirming that the assignments are within 3° in χ_1 and 10° in χ_2 of the previous characterization (*2*). This is despite the refinement of the polypeptide backbone and a changed sign for two of the quadrupolar splittings. For the analogues, the rmsd values are not as low and two solutions exist. The increased rmsd clearly reflects the more significant assumptions that have been made: that the molecular dynamics are the same as those in gA and that the tensors and/or molecular structure (of the indole) are unchanged by fluorination. Consequently, rmsd values of 3−10 kHz are not unreasonable. For all sites in DMPC and DOPC except 6F-Trp_{11} in DMPC, the χ_2 values near 270° represent the lowest rmsd values, again consistent with energetic conformational search results (*43*). By exclusion from the 6F-Trp_{11} map analysis of the para deuteron adjacent to the fluorine, ζ_2 (i.e., the most suspect deuteron for a changed tensor), a lower rmsd in the vicinity of a χ_2 of 270° compared to that near 310° is achieved. Therefore, a χ_2 near 270° for 6F-Trp_{11} has been chosen as most probable, consistent with the Trp_{11}-gA orientation and as suggested by the simple comparison of the ^2H spectra for the two side chains. The values of χ_1 and χ_2 at the center of the minima are summarized in Table 3 for this conformation along with the corresponding rmsd.

Clearly, the conformations of the side chains are not substantially affected by fluorination, but even small changes

Table 3: Torsion Angles and Root-Mean-Square Deviations[a] for the Indole Rings and Fluorinated Tryptophans in Gramicidin A and Fluorotryptophan Gramicidins

	DMPC					
	Trp_{11}	5F-Trp_{11}	6F-Trp_{11}	Trp_{13}	5F-Trp_{13}	6F-Trp_{13}
χ_1	289	289	290	296	300	296
χ_2	269	276	272	275	263	274
rmsd	0.6	5.4	7.0	1.0	3.1	3.6

	DMPC		
	Trp_{15}	5F-Trp_{15}	6F-Trp_{15}
χ_1	299	294	300
χ_2	270	274	271
rmsd	0.6	4.8	4.8
χ_1		292	
χ_2		301	
rmsd		8.3	

	DOPC		
	Trp_{13}	5F-Trp_{13}	6F-Trp_{13}
χ_1	296	299	296
χ_2	272	261	272
	2.0	3.1	2.7
χ_1	294	296	295
χ_2	310	321	314
	8.0	13.0	3.7

[a] The root-mean-square deviation (rmsd) is determined as described in Materials and Methods. It corresponds to the difference between observed and calculated orientational constraints for the deuterons of the indole ring.

can significantly affect the magnitude of the various dipole components. In fact, these values remain small compared to the amplitude of the librational motions about χ_2 that are on the order of ± 20 to $\pm 30°$ for the Trp side chains of gA (*37*). Furthermore, it is clear for sites 11, 13, and 15 presented here that 5-fluorination has a greater effect on the side chain torsion angles than 6-fluorination.

DISCUSSION

Figures 2−4 show that high-resolution orientational constraints are available from ^2H solid state NMR spectra of sites 11, 13, and 15. The fluorination of Trp at these positions has not influenced the propensity of this molecule to insert and align parallel to the bilayer normal. Indeed, conductance measurements clearly show that for various 5F-Trp analogues, including 5F-Trp_9-gA, the channel state is formed in membranes (*35*, *38*). The ^{15}N backbone chemical shifts (Table 1) indicate that the backbone has not been affected significantly by fluorination of the indoles or by the use of DOPC instead of DMPC.

Assignment of the ^2H Splittings and the Choice of qcc. To analyze the orientational constraints, it is essential to make accurate assignments. Moreover, the sign of the quadrupolar splitting needs to be determined and reasonable assumptions about the motional averaging of the tensors made. ^{15}N and ^{19}F doubly labeled tryptophan was not available for accurately characterization of the dynamics, and therefore, the dynamics were assumed to be the same as in gA. The similarity of the analogue orientations achieved while using this assumption justifies its use. Numerous sign combinations for the quadrupolar splittings were investigated, and the correct combination was chosen on the basis of the minimal rmsd in the χ_1/χ_2 plots. Finally, it was also assumed that the static quadrupolar tensors were the same as in gA and that they were not distorted by the presence of fluorine. While this is likely to be the weakest assumption and the one responsible for increased rmsd in fluorinated analogues, it is not a bad assumption. The maximum difference in quadrupolar splitting between ϵ_3 and ζ_2 is only 14 kHz, the equivalent of just a 2.3° difference in orientation, if interpreted as a purely structural change. Therefore, it is reasonable, on the basis of small but significant changes in the partial charge distribution (Figure 1) in the fluorinated analogues, that the quadrupolar tensors will be slightly distorted. From the crystal structure of the F-indole analogues, it does not appear to be due to structural changes induced by the fluorine (*7*). This distortion was not quantitated for the analysis presented here, because of its small magnitude. The initial assignments were aided both by observations in DOPC and by the observed $^{19}F-^2H$ dipolar interactions. By simple comparison of the spectra with the assigned gA spectra and with the available $^{19}F/^2H$ dipolar observations, tentative assignments are made that include a sign ambiguity for the para deuterons. The computations of contour plots (Figure 5) are used to define a final set of assignments for each fluoro-Trp side chain.

Here the calculated rmsds included both para deuterons. The constraints could be judged redundant in the sense that the two C−D bonds are almost parallel. Indeed, Koeppe et al. (*42*) treated the two splittings as a single constraint calculated from their average. However, here, the presence of the fluorine appears to affect the ^2H tensor as mentioned above, and this effect is expected to be greater for deuterons closer to the fluorine. Since only one of the para deuterons is close to a fluorine (ϵ_3 in 5F-Trp and ζ_2 in 6F-Trp), the change in the ^2H tensor upon fluorination is expected to be larger for one of the splittings compared to the other. It is therefore not appropriate to average the two observed splittings. Our strategy, which allows for a check on individual values of $\Delta\nu_{cal} - \Delta\nu_{obs}$, indicates that the deuterons closer to the fluorine have higher variance from calculated values than the other sites when comparisons are made at the local minima of the contour plots. Despite this increased variance, both splittings have been included in the rmsd calculations.

Structural Effects of the Fluorination. The spectra obtained for position 9 indicated that 5- and 6-fluorination induce microheterogeneity in the samples, especially for 5F-Trp-gA. The literature presents two possible conformations for this side chain (*2*, *42*, *43*), both of which are consistent with the solid state NMR data. However, since the ^{15}N backbone chemical shifts of 5F-Trp_9 analogues are similar to gA and are well defined, the instability is probably due to a slight perturbation in the side chain conformation, rather than to a change in the rotameric state. Indeed, the range may be less than 5°, but it is enough to cause resonance overlap and an inability to quantitatively analyze the data in this particular case. Position 9 lying deeper in the bilayer than positions 11, 13, and 15 is located in an environment with a dielectric constant that is lower than those of the other Trp side chains. The electronegative fluorine in this environment may destabilize the side chain conformation, or the very large dipole moment may not be stable in this environment. Indeed, 5F-Trp has a larger dipole moment than 6F-Trp, consistent with the observed increase in the level of disorder. Moreover, 5F-

Table 4: Geometric and Electrostatic Parameters Associated with the Most Stable Tryptophan Conformations of Tryptophans and Fluorinated Tryptophan in the Gramicidin Channels

	Trp_{11}	5F-Trp_{11}	6F-Trp_{11}	Trp_{13}	5F-Trp_{13}	6F-Trp_{13}	Trp_{15}	5F-Trp_{15}	6F-Trp_{15}
				Critical Distances (Å)					
r_i	11.9	12.0	11.9	12.4 12.4[a]	12.2 12.3[a]	12.4 12.4[a]	13.4	13.6	13.3
$r_\perp$	8.1	8.2	8.1	8.0 8.0[a]	7.8 7.8[a]	8.0 8.0[a]	7.4	7.5	7.4
r_{NH}	11.4	11.4	11.3	12.1 12.1[a]	11.8 11.9[a]	12.1 12.1[a]	13.8	14.0	13.7
r_F[b]/$r_{H\zeta 3}$[c]/$r_{H\eta 2}$[d]	5.9[c]/7.6[d]	5.8[b]	7.5[b]	6.4[c]/7.9 6.5[a,c]/8.0[a,d]	6.5[b] 6.6[a,b]	7.9[d] 8.0[a,d]	8.1[c]/9.5[d]	7.9[a,b]	9.3[b]
				Critical Orientations (deg)					
θ_i	43	43	43	40 40[a]	40 40[a]	40 40[a]	34	33	34
θ_{NH}	33	41	33	38 41[a]	45 46[a]	38 39[a]	42	44	41
θ_μ	22	18	39	18 20[a]	26 28[a]	31 32[a]	19	15	28
				Dipole Components (D)					
$\mu_{\|\|}$	2.0	3.8	2.4	2.0 2.0[a]	3.6 3.5[a]	2.6 2.6[a]	2.0	3.9	2.7
$\mu_\perp$	0.8	1.2	1.9	0.6 0.7[a]	1.7 1.9[a]	1.6 1.6[a]	0.7	1.0	1.4
μ_i	1.7	2.9	1.1	1.9 1.9[a]	3.5 3.5[a]	1.6 1.6[a]	2.0	3.5	1.9
μ_r	0.5	0.2	−0.9[e]	0.6 0.6[a]	1.2 1.2[a]	−0.7[e] −0.6[a,e]	0.7	0.5	−0.5[e]
μ_t	0.6	1.2	1.7	0.3 0.3[a]	1.3 1.4[a]	1.4 1.5[a]	0.2	0.9	1.3
				Conductance in DOPC and DPhPC[f] (pA)					
DOPC/decane				2.02 ± 0.03	2.55 ± 0.03				
DPhPC/decane				2.11 ± 0.03	2.50 ± 0.04				

[a] The values for positions 11 and 15 are from DMPC (1/8) samples. For position 13, the first value is from DMPC samples and the second value from DOPC (1/25) samples. [b] Distance from the fluorine in the fluorinated tryptophans to the bilayer center. [c] Distances from $H_{\zeta 3}$ hydrogens (in tryptophan) to i. $H_{\zeta 2}$ and $H_{\eta 2}$ are the positions occupied by fluorine in 5F-Trp and 6F-Trp, respectively, so that values denoted with footnote b can be compared to values denoted with footnote c in 5F-Trp-gA and to values denoted with footnote d in 6F-Trp-gA. [d] Distances from $H_{\eta 2}$ hydrogens (in tryptophan) to i. $H_{\zeta 2}$ and $H_{\eta 2}$ are the positions occupied by fluorine in 5F-Trp and 6F-Trp, respectively, so that values denoted with footnote b can be compared to values denoted with footnote c in 5F-Trp-gA and to values denoted with footnote d in 6F-Trp-gA. [e] A negative sign means that the vector points toward the channel center. [f] Conductances measured in 1 M KCl with a membrane potential of 100 mV and at 23 °C (*35*).

Trp-gA positions the fluorine further into the bilayer than 6F-Trp-gA.

Microheterogeneity may arise from a number of sources. Aggregation could affect side chain positions and may be induced by burying a significant dipole or electronegative atom in such a low-dielectric environment. However, only a slight improvement in the resonance line widths was observed upon dilution in DMPC (1:35) or DOPC (1:25). More likely, this microheterogeneity results from destabilizing the Trp_9 minimum energy conformation to the extent that other conformational substates have approximately the same energy. This suggests a convoluted potential energy surface with many tightly spaced conformational substates with approximately equal energies.

This is not the first time that substitution at position 9 has generated more complex structural and functional effects compared to substitutions at positions 11, 13, and 15. Hinton and co-workers (*44*) investigated the structural effects of substituting glycine (Gly) for Trp in gA. The studies, carried out in SDS micelles, showed that Gly substitution at position 9 was responsible for more structural heterogeneity than Gly substitution at positions 11, 13, and 15. Becker et al. (*34*) showed that the Trp to Phe substitution in gA that affected conductance most was the substitution at position 9. It will be interesting to carefully examine single-channel currents of fluorinated Trp_9-gA for evidence of diversity in the side chain orientation. However, this observed microheterogeneity at position 9 may not significantly affect channel conductance, because of its small angular range of disorder. In fact, a cursory examination of conductance measurements indicates that the process causing line broadening in 5F- and 6F-Trp_9-gA does not dramatically affect the channel current noise or conductance state dispersity (*38*; D. Busath, unpublished results).

In the comparison of the side chain conformations at a given position (Table 3), the changes in χ_1 are very minor and changes in χ_2 are small, but significant (as much as 12°). On the basis of the fit of the predicted and observed quadrupolar splittings, an rmsd of 7 kHz is approximately equal to an error of ±2° in this time-averaged structural determination. Consequently, on the basis of the precision of the NMR data, many of the χ_2 differences are indeed structurally significant. The indole $N_{\epsilon 1}$−H positions and orientations relative to the interface remain similar (Table 4) and typical of indoles in various membrane proteins, including the photosynthetic reaction center (*45*, *46*) and cytochrome *c* oxidase (*47*). The reasons for such an orientation at the interface have been the subject of various studies, but it is still unclear whether it is primarily due to the hydrogen bonding potential of the $N_{\epsilon 1}$−H at the interface, interaction of the side chain dipole moment with the interfacial dipole potential, or steric constraints imposed by

the backbone structure. White and co-workers (*48*) have also pointed out the potential of the ring quadrupole moment and its flat shape. The location of N_{ϵ_1}-methylindole has also been found at the interface, and this has been used to suggest that hydrogen bonding at the interface is not the primary reason for the Trp side chain orientational preference (*49*). Here we find that substantial modification of the indole dipole moment and orientation does not dramatically affect the $N_{\epsilon_1}-H$ bond orientation.

When the tryptophans in gramicidin are modified with fluorine, structural modifications are induced, especially in 5F-Trp where the changes in dipole magnitude are greater and where the electronegative atoms are buried deeper in the bilayer interstices. From the data for positions 11, 13, and 15, there is an opportunity to assess whether these changes are in response to minimizing the dipole-generated electric field penetration or penetration of the electronegative fluorine into the bilayer interstices. However, as seen in Table 4, the structural modifications do not appear to minimize either of these energetic considerations. Thus, it suggests that the tryptophans of gA reside in very favorable bilayer locations and orientations such that the structural modifications are minimal.

Functional Implications. The indoles have several functional roles in the gramicidin channel. The dipoles are important for the efficiency of the cation conductance (*2*, *34*, *38*). They are also responsible for the stability of the single-stranded versus double-stranded conformations (*23*−*32*) as well as being responsible for the orientation of the channel with respect to the bilayer (*25*). Moreover, the indoles may play an important role in defining the channel's helical sense (*36*; M. Cotten et al., unpublished results). These features have to do with hydrogen bonding potential, and the significant side chain dipole. Increasing the dipole and changing its orientation have not substantially destabilized the structure or its orientation with respect to the bilayer. However, introduction of 5F-Trp is known to modify the conductance of this channel (*35*, *38*). Experiments with 6F-Trp analogues currently underway indicate that they, too, have modified conductances.

The influence of the dipoles on function is presented here by calculating various dipole components and comparing them with those of gA (Table 4) as illustrated in Figures 6 and 7. The distances are pictured on the gramicidin A dimer in Figure 6A. r_i is the distance between the point "i" on the channel axis at the center of the bilayer and the center of geometry of heavy atoms of the indole ring. $r_\perp$ is the distance between the center of the Trp ring and the channel axis in a plane parallel to the bilayer surface. r_{NH} represents the distance between the indole $N_{\epsilon_1}-H$ proton and the center of the bilayer, while r_F represents the distance between fluorine and the center of the bilayer. μ is the indole dipole moment (Figure 6B), split in three components: axial or parallel to the channel axis ($\mu_{||}$), perpendicular to the channel axis ($\mu_\perp$), and parallel to the r_i direction (μ_i). Furthermore, $\mu_\perp$ is broken down into radial μ_r and tangential μ_t components (Figure 6C).

Sancho and Martinez (*50*) have used a macroscopic (continuum) approach to describe the effect of a ring of dipoles near the channel mouth. When using a ring of dipoles oriented parallel to the channel axis, the potential energy surface features a minimum at "i" that decreases the energy

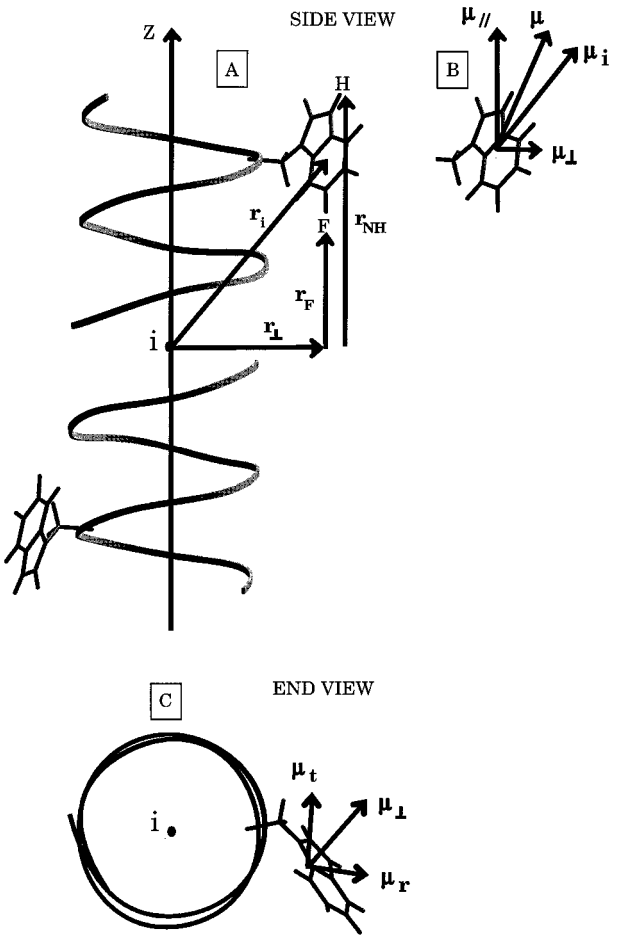

FIGURE 6: Critical parameters characterizing the role of the indole dipole moment in channel function are defined. A side view (A) of a gA channel dimer and the corresponding end view (C) of the channel top monomer are shown with the most probable Trp_{11} conformation (*2*). (A) "i" is a point on the channel axis (Z) at the bilayer center. r_i is the distance between the center of geometry of the heavy atoms of the indole ring and the point "i". r_{NH} is the distance between the hydrogen of the indole NH group and the center of the bilayer. $r_\perp$ is the distance between the center of the indole ring and the channel axis in a plane parallel to the bilayer surface. r_F is the distance between the fluorine and the bilayer center. (B) μ is the dipole moment in the plane of the indole ring, and $\mu_{||}$ and $\mu_\perp$ are its components parallel to the channel axis and perpendicular to it, respectively. Also shown is the component parallel to r_i. (C) $\mu_\perp$ is decomposed into components, radial (μ_r) and tangential (μ_t) with respect to the channel axis.

barrier at "i" for ion translocation. Note that the effects of two rings of dipoles located near each channel entrance in a symmetric channel do not cancel each other. This is possible because the polarization of the water bath renders the side chain dipole comparable to a negative point charge that yields a negative interaction energy with the cation, even at the center of the channel. Also, the negative ends of the dipoles at the two ends of the channel are additive, whereas the positive ends are more distant and contribute less to the potential profile (*43*). A ring of radial dipoles, in contrast to axial ones, yields a potential energy surface with two minima near the channel entrances. This suggests that the radial components should affect cation binding as opposed to translocation. To explain the conductance studies of analogues, Sancho and Martinez (*50*) observed that the energy for the interaction between the axial component of the indole dipole moment and the cation at the center of the channel is

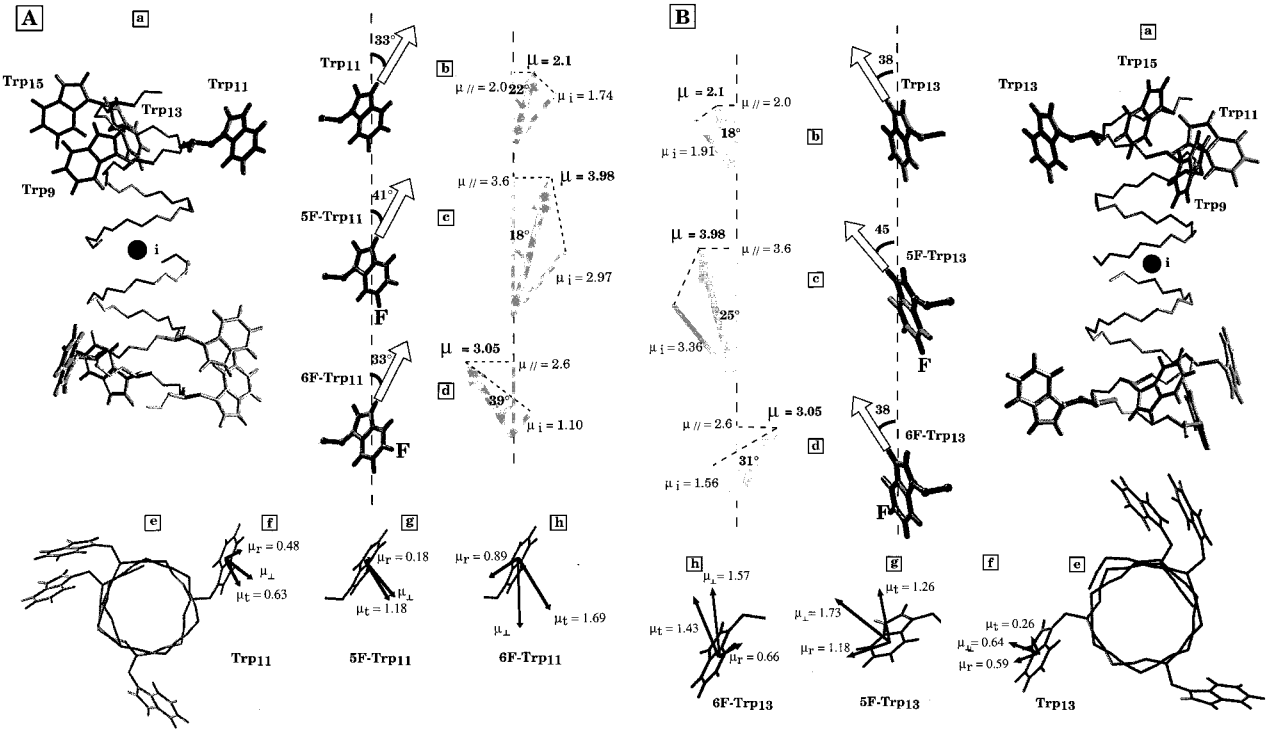

FIGURE 7: Critical parameters characterizing the role of the indole dipole moment on channel function (Figure 6) are highlighted for positions 11 (A) and 13 (B) in DMPC. Two side views (a) of a gA channel dimer and the corresponding end views (e) of the channel monomer shown with the most probable Trp_{11} and Trp_{13} conformations are used to make comparisons with the most probable 5F-Trp and 6F-Trp side chain conformations (this study, Table 3) shown as insets near the gA structure. For each indole (b), 5F-Trp (c), and 6F-Trp (d) highlighted in the top monomer, the magnitude and direction of the dipole moment components parallel ($\mu_{||}$) and perpendicular ($\mu_{\perp}$) to the channel axis and along the direction of the vector pointing from the center of the channel to the center of mass of the indole ring (μ_i) are represented in the plane containing the dipole moment μ. The orientation of the dipole moment and N_{ϵ_1}−H group with respect to the channel axis has also been added. $\mu_{\perp}$ has been decomposed into components, radial (μ_r) and tangential (μ_t) with respect to the channel axis for Trp (f), 5F-Trp (g), and 6F-Trp (h). Note that the most probable Trp_9 conformation characterized by Arseniev et al. (*22*) and suggested by Koeppe et al. (*42*) has a χ_1 value close to 90° vs 270° as shown here and by Hu and Cross (*2*).

stabilizing. However, they explained different conductance behaviors among various gA analogues by considering the radial component of the dipole moment of the tryptophan side chain(s). They concluded that optimal effects on channel conductance of the Trp radial dipole moment components would be achieved for indole rings oriented perpendicular to the bilayer normal. This contrasts with the interpretation of solid state NMR-determined axial components and conductance data (*2*, *35*). For a broad collection of Trp to Phe substitutions in gA, a linear relationship between the sum of the interaction energy between monopole (cation at "i") and dipoles μ_i (Trp residues) and the natural log of conductance has been noted (*2*). Not only does this demonstrate the influence of long-range electrostatic interactions on function, but it also suggests that, in this lipid environment, the rate-limiting step is at the bilayer center, "i". This is not to say that the radial components are not important for cation binding. Indeed, Hu and Cross (*2*) have suggested that the tangential components may also be important for facilitating cation movement, since evidence has been published suggesting that the cations move through the channel on a helical path (*51*, *52*).

It is clear from Table 4 that, for a given side chain, r_i remains quasi constant. For the calculation of the monopole−dipole interaction energy, the μ_i component has been calculated reflecting both the change in dipole orientation with respect to the ring and the modified orientation of the rings such as 5F-Trp_{11}-gA and 5F-Trp_{13}-gA. The dipole component, μ_i, that influences the potential energy barrier at "i" is substantially larger in 5F-Trp-gA than in gA for each of the three positions that are characterized. This is consistent with the 26 and 18% increase in conductance for 5F-Trp_{13}-gA in DOPC/decane and DPhPC/decane, respectively (Table 4) (*35*). While the increase in μ_i is significant, it is not enough to compensate for the loss of Trp_9 in 5F-Trp_{11},Phe_9-gA for which Andersen and co-workers showed a reduction in conductance in DPhPC/decane (*38*). It is predicted on the basis of the results presented here that for 6F-Trp-gA a reduction in conductance could be anticipated, especially for 6F-Trp_{11}-gA, while for 6F-Trp_{15}-gA the reduction is expected to be insignificant.

The dipole component μ_r that influences cation binding is also substantially influenced by fluorination. 5F-Trp_{13}-gA exhibits a substantial increase in this component that should lead to stabilization of the cation in the binding site. All the 6F-Trp-gA analogues, however, show a reversal in this component, and consequently, cation dissociation constants are predicted to be higher for these analogues.

It has been suggested (*2*) that the tangential component of the dipoles could be important in conductance since the conductance pathway is on a helical path through the channel. For all 5F-Trp and 6F-Trp gramicidin A analogues, the tangential components are substantially greater. Potentially, this could result in destabilization of the cation in the binding site or further delocalization of the binding site (*52*).

Electrostatic interactions over distances as great as 12−13 Å have considerable functional significance in bilayer environments as shown with these and previous studies of gramicidin. Recently, with the structure of the potassium channel from *Streptomyces lividans*, the potential of such electrostatic interactions has also been suggested, not with indoles, but with the dipoles of α−helices (*1*). Four helices at a tilt of approximately 45° with respect to the bilayer normal are oriented toward the very center of the bilayer on a cation pathway. The results presented here help illuminate and define the experimental and theoretical steps that will be required to interpret the effects of these helical dipoles on channel conductance. In gramicidin A, it is clear that the functional sensitivity to the orientation and magnitude of the side chain dipoles makes it imperative that high-resolution structural characterization be realized before structure−function correlations such as those demonstrated here can be achieved.

ACKNOWLEDGMENT

We are indebted to the staff of the Florida State University NMR facility, J. Vaughn, R. Rosanske, and T. Gedris, for their skillful maintenance and service of the spectrometers and H. Henricks and U. Goli of the Bioanalytical Synthesis and Services Facility for their expertise and maintenance of the ABI 430A peptide synthesizer and HPLC equipment. We thank Prof. Giulano Alagona (CNR, Pisa, Italy) for sending us the Merz-Kollman 6-31G* partial charges for the fluorinated indoles.

REFERENCES

1. Doyle, D. A., Morais Cabral, J. M., Pfuentzer, R. A., Kuo, A., Gulbis, J. M., Cohen, S. L., Chait, B. T., and MacKinnon, R. (1998) *Science 280*, 69−77.
2. Hu, W., and Cross, T. A. (1995) *Biochemistry 34*, 14147−14155.
3. Cowley, E. G., and Partington, J. R. (1936) *J. Chem. Soc.*, 47−50.
4. Janetzky, E. F. J., and Lebret, M. C. (1944) *Rec. Trav. Chim. Pays-Bas 63*, 123−126.
5. Weiler-Feilchenfeld, H., Pullman, A., Berthod, H., and Geissner-Prettre, C. (1970) *J. Mol. Struct. 6*, 297−304.
6. Lumbroso, H., and Pappalardo, G. (1961) *Bull. Soc. Chim. Fr.*, 1131−1135.
7. Antolic, S., Kojicprodic, B., Tomic, S., Nigovic, B., Magnus, V., and Cohen, J. D. (1996) *Acta Crystallogr. B 52*, 651−661.
8. Pa'rka'nyi, C., Oruganti, S. R., Abdelhamid, A. O., and Szentpa'ly, L. V. (1986) *THEOCHEM 135*, 105−116.
9. Alagona, G., Ghio, C., and Monti, S. (1998) *THEOCHEM 433*, 203−216.
10. Tomic', S., van Duijneveldt, F. B., Kroon-Batenburg, L. M., and Kojic'-Prodic', B. (1995) *Croat. Chem. Acta 68*, 205−214.
11. Westbrook, J. D., Levy, R. M., and Krogh-Jesperson, K. (1992) *J. Comput. Chem. 8*, 979−989.
12. Simonson, T., Wong, C. F., and Brünger, A. T. (1997) *J. Phys. Chem. A 101*, 1935−1945.
13. Levine, I. N. (1991) *Quantum Chemistry*, 4th ed., p 476, Prentice Hall, Englewood Cliffs, NJ.
14. Reed, A. E., Curtiss, F., and Weinhold, F. (1988) *Chem. Rev. 88*, 889−926.
15. Breneman, C. M., and Wiberg, K. B. (1990) *J. Comput. Chem. 11*, 361−373.
16. Bayly, C. I., Cieplak, P., Wornell, W. D., and Kollman, P. A. (1993) *J. Phys. Chem. 97*, 10269−10280.
17. Gastieger, J., and Marsili, M. (1980) *Tetrahedron 36*, 3219−3228.
18. Rappe, A. K., and Goddard, W. A. (1991) *J. Phys. Chem. 95*, 3358−3363.
19. Ketchem, R., Hu, W., and Cross, T. (1993) *Science 261*, 1457−1460.
20. Ketchem, R. R., Roux, B., and Cross, T. A. (1997) *Structure 5*, 1655−1669.
21. Arseniev, A. S., Lomize, A. L., Barsukov, I. L., and Bystrov, V. F. (1985) *FEBS Lett. 186*, 168−174.
22. Lomize, A. L., Orekhov, V. Y., and Arseniev, A. S. (1992) *Bioorg. Khim. 18*, 182−200.
23. Hu, W., Lee, K.-C., and Cross, T. A. (1993) *Biochemistry 32*, 7035−7047.
24. Arumugam, S., Pascal, S., North, C. L., Hu, W., Lee, K. C., Cotten, M., Ketchem, R. R., Xu, F., Brenneman, M., Kovacs, F., Tian, F., Wang, A., Huo, S., and Cross, T. A. (1996) *Proc. Natl. Acad. Sci. U.S.A. 93*, 5872−5876.
25. O'Connell, A. M., Koeppe, R. E., II, and Andersen, O. S. (1990) *Science 250*, 1256−1259.
26. Durkin, J. T., Providence, L. L., Koeppe, R. E., II, and Andersen, O. S. (1992) *Biophys. J. 62*, 145−159.
27. Van Mau, N., Bonnet, B., Benayad, A., and Heitz, F. (1994) *Eur. Biophys. J. 22*, 447−452.
28. Salom, D., Bañó, M. C., Braco, L., and Abad, C. (1995) *Biochem. Biophys. Res. Commun. 209*, 466−473.
29. Seoh, S. A., and Busath, D. (1995) *Biophys. J. 68*, 2271−2279.
30. Cotten, M., Xu, F., and Cross, T. A. (1997) *Biophys. J. 73*, 614−623.
31. Salom, D., Perez-Paya, E., Pascal, J., and Abad, C. (1998) *Biochemistry 37*, 14279−14291.
32. Cotten, M., Fu, R., and Cross, T. A (1999) *Biophys. J. 76*, 1179−1189.
33. Killian, J. A. (1992) *Biochim. Biophys. Acta 1113*, 391−425.
34. Becker, M. D., Greathouse, D. V., Koeppe, R. E., II, and Andersen, O. S. (1991) *Biochemistry 30*, 8830−8839.
35. Busath, D., Thulin, C. D., Hendershot, R. W., Revell Phillips, L., Maughan, P., Cole, C. D., Bingham, N. C., Morrison, S., Baird, L. C., Hendershot, R. J., Cotten, M., and Cross, T. A. (1998) *Biophys. J. 75*, 2830−2844.
36. Koeppe, R. E., II, and Andersen, O. S. (1996) *Annu. Rev. Biophys. Biomol. Struct. 25*, 231−258.
37. Hu, W., Lazlo, N. D., and Cross, T. A. (1995) *Biochemistry 34*, 14138−14146.
38. Andersen, O. S., Greathouse, D. V., Providence, L. L., Becker, M. D., and Koeppe, R. E., II (1998) *J. Am. Chem. Soc. 120*, 5142−5146.
39. Fields, G. B., Fields, C. G., Petefish, J., Van Wart, H. E., and Cross, T. A. (1988) *Proc. Natl. Acad. Sci. U.S.A. 85*, 1384−1388.
40. Fields, C. G., Fields, G. B., Noble, R. L., and Cross, T. A. (1989) *Int. J. Pept. Protein Res. 33*, 298−303.
41. Subramanian, E., and Sahayamary, J. J. (1989) *Int. J. Pept. Protein Res. 34*, 134−138.
42. Koeppe, R. E., II, Killian, J. A., and Greathouse, D. V. (1994) *Biophys. J. 66*, 14−24.
43. Dorigo, A. E., Anderson, D. G., and Busath, D. D. (1999) *Biophys. J. 76*, 1897−1908.
44. Hinton, J. F., Wahburn-McCain, A. M., Snow, A., and Douglas, J. (1997) *J. Magn. Reson. 124*, 132−139.
45. Michel, H., and Deisenhofer, J. (1990) *Curr. Top. Membr. Transp. 36*, 53−69.
46. Steffen, M. A., Lao, K., and Boxer, S. G. (1994) *Science 264*, 810−816.
47. Tsukihara, T., Aoyama, H., Yamashita, E., Tomizaki, T., Yamaguchi, H., Shinzawa-Itoh, K., Nakashima, R., Yaono, R., and Yoshikawa, S. (1996) *Science 272*, 1136−1144.
48. Yau, W.-M., Wimley, W. C., Gawrisch, K., and White, S. H. (1998) *Biochemistry 37*, 14713−14718.
49. Persson, S., Killian, J. A., and Lindblom, G. (1998) *Biophys. J. 75*, 1365−1371.
50. Sancho, M., and Martinez, G. (1991) *Biophys. J. 60*, 81−88.
51. Jordan, P. C. (1990) *Biophys. J. 58*, 1133−1140.
52. Tian, F., and Cross, T. A. (1998) *J. Mol. Biol. 285*, 1993−2003.

BI982981M